Geochemistry Geophysics Geosystems G3
AN ELECTRONIC JOURNAL OF THE EARTH SCIENCES
Published by AGU and the Geochemical Society

Article
Volume 9, Number 3
8 March 2008
Q03008, doi:10.1029/2007GC001863
ISSN: 1525-2027

Production of brief extreme ground acceleration pulses by nonlinear mechanisms in the shallow subsurface

Norman H. Sleep and Shuo Ma

Department of Geophysics, Stanford University, 397 Panama Mall, Stanford, California 94305, USA (norm@stanford.edu)

[1] A brief pulse of extreme acceleration ~20 m s^{-2} was recorded at Station FZ16 during the 2004 M_w 6.0 Parkfield, California, earthquake. The sustained acceleration at the dominant frequency is a factor of ~2 below the maximum. Here we show that the pulses of extreme acceleration might originate in the shallow subsurface, rather than on the main fault plane. Two nonlinear mechanisms can feasibly convert low-frequency energy of the incident wave into high-frequency pulses with extreme acceleration: (1) Dynamic stress carried by strong seismic waves causes small shallow cracks to slip in secondary earthquakes. (2) The elasticity of the shallow subsurface is nonlinear. The relationship between dynamic shear stress and strain is linear at small strains. At the large strains associated with strong ground motion, shear deformation locks compliant cracks by bringing their asperities into contact. The locking increases the instantaneous shear modulus of the cracked rock. Computations indicate that both mechanisms produce high accelerations in the later part of the strong ground motion. These testable hypotheses imply that brief pulses of extreme acceleration are likely not a property of the main fault and hence not harbingers of prolonged pulses of extreme acceleration.

Components: 4881 words, 10 figures.

Keywords: strong ground motion; Parkfield earthquake; triggered earthquakes; site response.

Index Terms: 7212 Seismology: Earthquake ground motions and engineering seismology; 4455 Nonlinear Geophysics: Nonlinear waves, shock waves, solitons (0689, 2487, 3280, 3285, 4275, 6934, 7851, 7852).

Received 22 October 2007; **Revised** 2 January 2008; **Accepted** 14 January 2008; **Published** 8 March 2008.

Sleep, N. H., and S. Ma (2008), Production of brief extreme ground acceleration pulses by nonlinear mechanisms in the shallow subsurface, *Geochem. Geophys. Geosyst.*, *9*, Q03008, doi:10.1029/2007GC001863.

1. Introduction

[2] Strong motion seismic instruments record brief pulses of extreme acceleration well over 1 g. Though these very brief pulses of high acceleration do not endanger most structures [e.g., *Kramer*, 1996, p. 68], they are of concern to engineers as they may indicate that more sustained pulses of high acceleration are possible. The purpose of this paper is to examine the physics of viable processes in the shallow subsurface away from the main fault that may cause extreme acceleration.

2. Observations

[3] The strong motion record at Station FZ16 for the 2004 M_w 6.0 Parkfield, California, earthquake (Figure 1) provides a well-resolved example of high acceleration [*Shakal et al.*, 2006]. The station

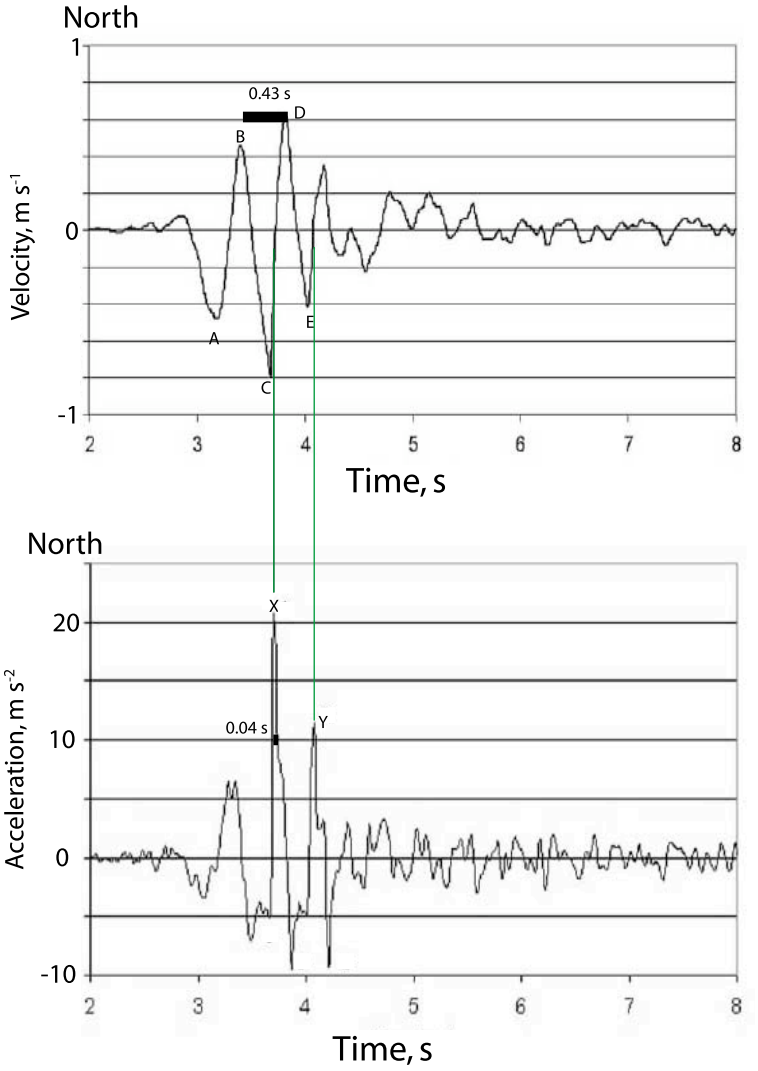

Figure 1. Northward particle (top) velocity and (bottom) acceleration from station FZ16 for the Parkfield earthquake, redrawn from the work of *Shakal et al.* [2006]. The maximum acceleration (X) occurs between velocity trough C and velocity peak D. The period between peaks B and D is 0.43 s. The maximum range in velocity is 1.4 m s^{-1}.

is about 1 km from the trace of the part of the San Andreas Fault that ruptured during this event.

[4] *Shakal et al.* [2006] discuss the validity of the FZ 16 record. The recording drum in the instrument rotated at an uneven rate but the measured acceleration behaved linearly during the strong shaking. *Shakal et al.* [2006] adjusted the raw records for this effect with the physical constraint that the acceleration integrated to no net velocity change. The gross variation of velocity (a maximum peak to peak change of 1.4 m s^{-1}), the peak acceleration (>20 m s^{-2}), and the dominant period of the velocity signal (0.43 s) are thus reliable.

[5] Note that sudden stick-slip in the mounting of a seismograph to the ground might cause brief accelerations. We consider this possibility unlikely for the site because the device might have ended up out of alignment. We thus seek causes within the shallow subsurface. This exercise is useful in general even if extreme accelerations observed near Parkfield were in fact recording artifacts.

2.1. Sustained Velocity and Acceleration

[6] An equivalent sine wave from the velocity seismogram describes well the sustained dominant-frequency part of the signal,

$$V = \frac{\Delta V}{2} \sin\left[\frac{2\pi t}{T}\right], \tag{1}$$

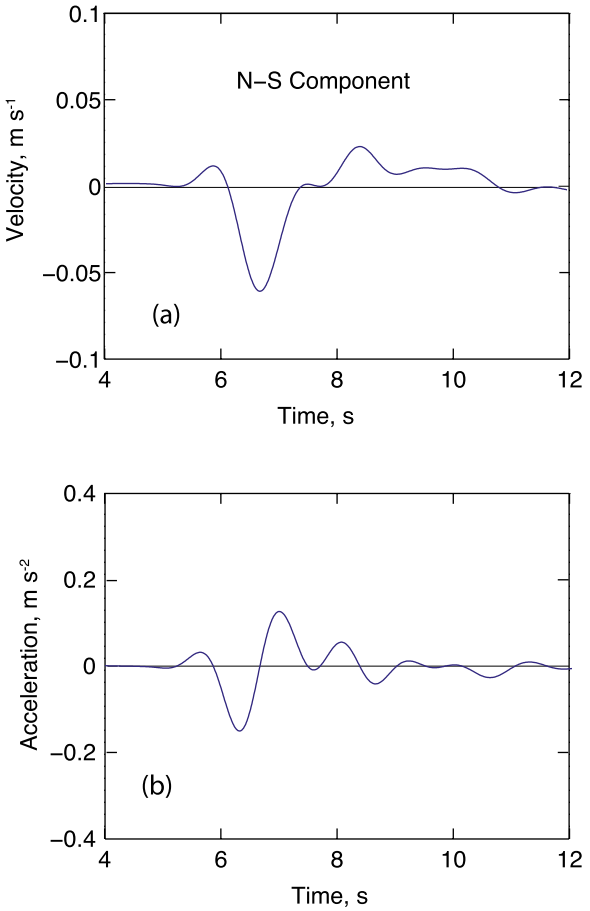

Figure 2. Predicted north-south (a) velocity and (b) acceleration for station FZ 16 from the preferred dynamic rupture model of *Ma et al.* [2008]. The dynamic rupture model resolves periods down to 1 s.

where ΔV is the velocity change over the strongest pulse, t is time, and T (0.43 s for the FZ 16 record) is the dominant period. The sustained acceleration is the maximum value of dV/dt,

$$a_{\text{sust}} = \frac{\pi \Delta V}{T}, \tag{2}$$

which is here 10.23 m s^{-2} or ~1 g for the record. That is, the recorded peak acceleration is more than twice the sustained acceleration.

2.2. Parkfield FZ 16 Site

[7] There does not seem do be any evident characteristic of the Station FZ 16 that would make one to expect exceptionally high accelerations there rather than at nearby stations. *Shakal et al.* [2006] point out that the accelerations recorded at this station for less intense shaking by other events are similar to those at nearby stations.

[8] There do not seem to be any untypical features in the shallow subsurface. The S-wave velocity in the shallow subsurface Vs30 is 339 m/s (National Center for Engineering Strong Motion Data tables). Thin alluvium covers sandstone beneath the station [*Shakal et al.*, 2006]. *Shakal et al.* [2006] reviewed other sites that experienced extreme acceleration. Many of them like FZ 16 are rock sites rather than thick soil sites.

2.3. Synthetic Seismogram for FZ 16

[9] With regard to the unremarkability of FZ 16, we obtain synthetic seismograms for the Parkfield event at this site. *Ma et al.* [2008] inverted strong motion data from 43 stations to infer the dynamic rupture process of the earthquake. They did not include FZ 16 in this inversion because no digital record of the strong motion is available.

[10] This dynamic rupture model provides a prediction of the shaking at FZ 16 that has the highest frequency of 1 Hz (Figure 2). The predicted record shows no evident resemblance to the actual record because most energy of the observed seismogram is above 1 Hz (Figure 1). The computed record does not have exceptionally high amplitude. We conclude from this "due diligence" exercise that the inversion does not give much information on brief high accelerations. We also conclude that the exercise gives no expectation that the shaking at FZ 16 would be particularly strong.

3. Site-Specific Causes for Extreme Accelerations

[11] Nonlinear mechanisms in the shallow subsurface can convert energy in the dominant lower-frequency part of the incident seismic wave into high-frequency energy. These processes greatly increase the maximum acceleration and weakly perturb the maximum velocity.

3.1. Generic Incident Pulse

[12] We assume a simple incident displacement pulse to illustrate the basic features of nonlinear behavior in the shallow subsurface (Figure 3). The pulse has the time dependence

$$D = D_0[1 - \cos(\omega t)], \tag{3}$$

over the time range of the pulse is $0 \leq t \leq 2\pi/\omega$, D_0 has dimensions of length and ω is angular frequency. The static displacement is zero at the

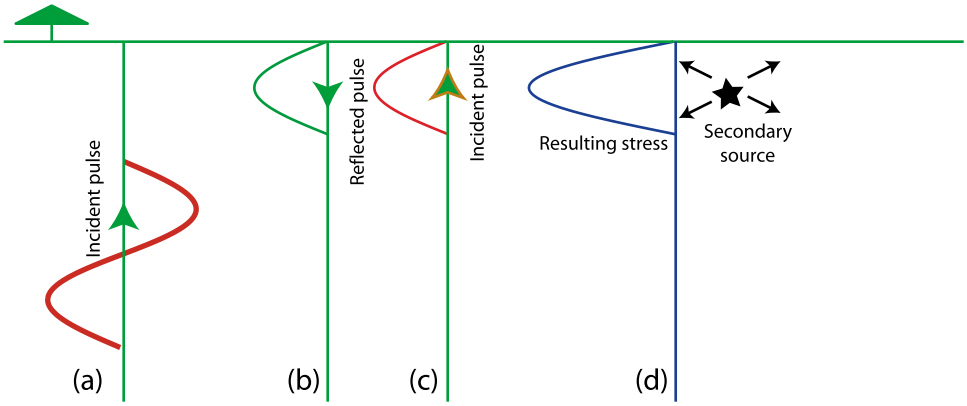

Figure 3. Reflection of simple pulse from the surface with dynamic shear stress as a function of depth. The stress at the quarter-wavelength depth is twice the maximum in the incident pulse. Secondary sources from nonlinear behavior occur at that time and depth. The energy from the secondary sources arrives at the surface late in the strong motion.

end of the pulse $t = 2\pi/\omega$ for simplicity. The particle velocity is thus

$$V = D_0\omega[\sin(\omega t)], \tag{4}$$

which is 0 at the start and end of the pulse. The dynamic acceleration is

$$a = D_0\omega^2[\cos(\omega t)]. \tag{5}$$

The acceleration suddenly changes to its maximum at the beginning and ending of the pulse, $t = 0, 2\pi/\omega$.

[13] Note that brief infinite accelerations as with a step-function change in dynamic velocity do not imply infinite energy or infinite dynamic stress. Rather the strain energy per volume of a wave in a whole space is equal to the kinetic energy per volume, $E = \tau^2/2G = \rho V^2/2$, where the relationship applies to S-waves, τ is the dynamic shear stress, G is shear modulus, and ρ is density [e.g., *Timoshenko and Goodier*, 1970, p. 491]. For example, the theoretical pulse from the work of *Brune* [1970] has brief unbounded acceleration at the start of the incident signal.

[14] Our pulse reflects from the free surface where the shear traction is zero (Figure 3). In the linear case, the maximum dynamic stress of twice that in the simple pulse occurs at the quarter-wavelength depth when the reflected first part of the pulse meets the upcoming second part of the pulse. We expect that nonlinear effects will be greatest when this occurs. Real or virtual secondary sources of high-frequency seismic energy from nonlinear behavior of the rock originate at this time. Hence the high-frequency energy arrives late in the strong ground motion. Note that the observed peak acceleration at FZ 16 occurs well after the start of strong motion as expected from this reasoning (Figure 1).

[15] We quantify two idealized dynamic mechanisms of viable physical processes that arise in the shallow subsurface rather than on the main fault plane. Both processes occur favorably in the shallow subsurface around the quarter-wavelength depth of the dominant period. The first involves secondary seismic events triggered by the dynamic stress in the strong incident seismic wave. The second involves elasticity where the shear stress does not depend linearly on shear strain. The rock contains compliant cracks. At low strains, these rock control the compliance of the rock mass. At large strains associated with strong ground motions, shear deformation of the crack brings asperities into contact. This locks the crack and increases the instantaneous shear modulus of the rock mass.

3.2. Shallow Triggered Seismicity

[16] *Fischer et al.* [2008] detected small high-frequency pulses for the 1999 Chi-Chi earthquake and A. D. Fischer et al. (Dynamic triggering of high-frequency bursts by strong motions during the 2004 Parkfield earthquake sequence, manuscript in preparation, 2008) discussed similar high-frequency events at shallow depths in the 2004 M_w 6.0 Parkfield earthquake. Both series of small events occurred during the arrival of strong seismic waves, which are probably caused by shallow faulting due to dynamic triggering. The lack of attenuation of high frequencies indicates a shallow source. Fischer et al. (manuscript in preparation, 2008) found that there is no correlation between events in Parkfield at stations as close as 50 m. This indicates that the

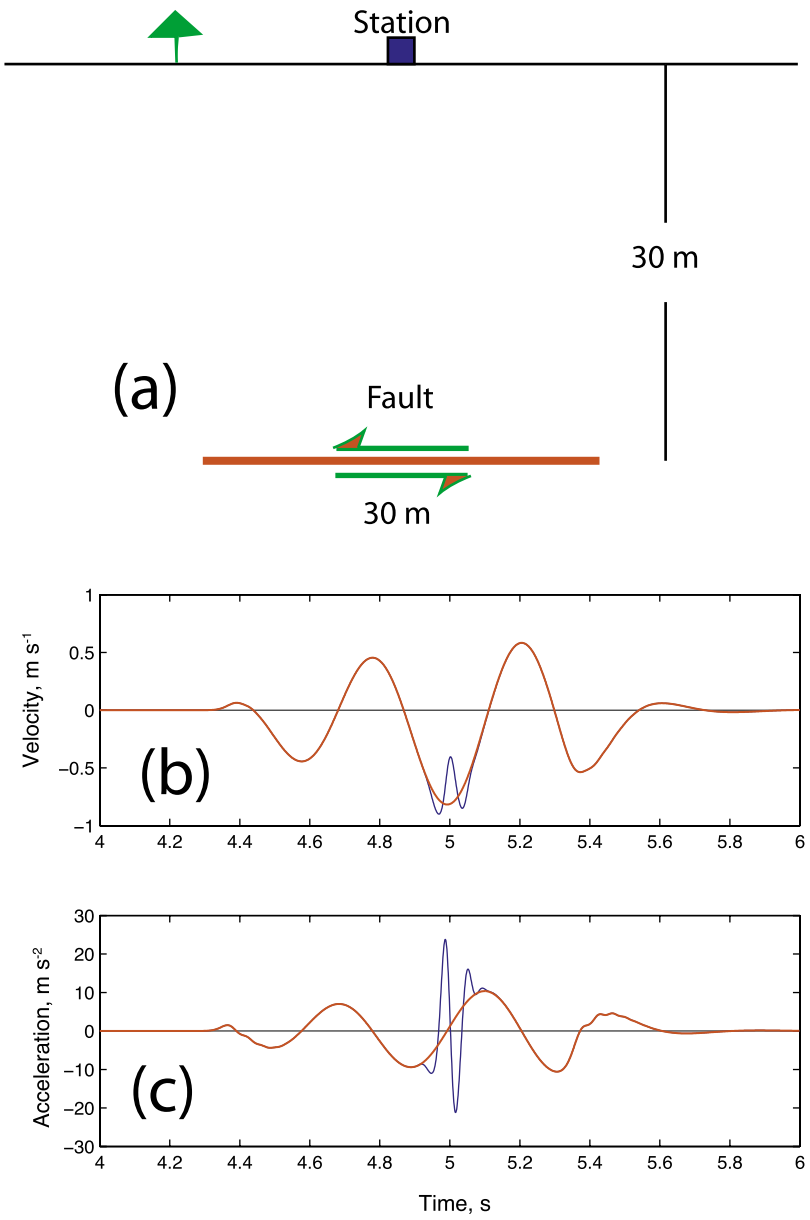

Figure 4. (a) The geometry of the two-dimensional fault and the station. Computed (b) particle velocity and (c) acceleration. The smooth curves are the linear response to the incident pulse and the effect of secondary rupture is around 5 s.

events were shallow and closer than that to the nearest recording station.

[17] The high-frequency events studied by *Fischer et al.* [2008; manuscript in preparation, 2008] are near the limit of detection. The wave amplitudes are small. Still the question arises whether dynamic stress carried by strong seismic waves and stick-slip on a joint or fracture could produce brief high accelerations. In analogy with a car, high accelerations will occur if a spring snaps when the car is oscillating.

[18] We again consider a vertically propagating SH-wave in a homogeneous half-space. The P wave velocity, S-wave velocity, and density of the material are 520 m/s, 300 m/s, and 2000 kg/m^3, respectively. We select a pulse of the incident wave that resembles that observed at FZ 16 but without strong acceleration (Figure 4).

[19] We impose a horizontal 30 m–long fault at 30 m depth within region and record synthetic seismograms above its center. The lithostatic stress is 0.6 MPa at this depth and the effective stress is

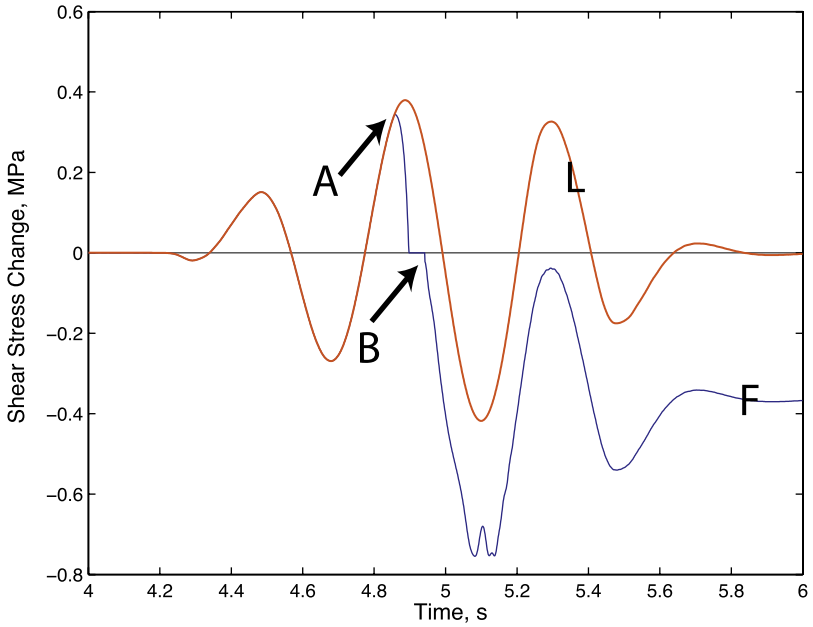

Figure 5. Computed stress change at the center of the fault plane for the incident linear pulse (L) and with faulting rupture (F). Slip begins at Point A. The fault slides at Point B at the dynamic friction, which is also the initial stress, and then locks. The slip leaves residual stress on the fault.

somewhat less than this depending on the depth to the water table. The initial shear stress is 0.05 MPa on the fault. Slip initiates at 0.394 MPa and the sliding stress drops to 0.05 MPa over a slip weakening distance of 0.015 m. Note the sliding frictional stress is equal to the initial stress such that the dynamic stress drop is zero. The energy released in the faulting entirely comes from the incident wave. A requirement of obtaining an extreme acceleration is that the slip weakening distance is small enough so that shear stress can drop completely from the static friction to the dynamic friction.

[20] We assume a mode 2 crack in a plane strain condition. We use 4-node rectangular elements everywhere to discretize the space and a central-difference scheme to discretize the time. The element size is 1 m and the time step is 0.001 s. The periodic boundary is implemented along the boundaries, except for the free surface, to simulate the plane wave. On the fault, we use a split-node scheme [*Andrews*, 1999]. Rupture occurs late when reflected waves from the free surface interact with upcoming waves. The shear stress on the fault drops to the sliding stress of 0.05 MPa soon after sliding begins (Figure 5). The fault locks immediately after the stress drops to the sliding friction due to the stopping phases from the fault boundaries (short fault length). The upcoming seismic wave supplies both energy for the fault to slide against friction and energy that leaves residual stresses and strains within the faulted material. That is, the shallow seismic event is a form of nonlinear attenuation, not an augmentation to the available seismic energy. A peak acceleration of 23.77 m/s^2 is successfully produced by the secondary rupture (Figure 4).

[21] We compute a second model with a 10-m wide fault at 10-m depth to give an indication of scaling to fault dimensions (Figure 6). We reduce the stress to initiate rupture on the fault, the initial stress and the sliding stress all by a factor of 3 on the assumption that these quantities scale with lithostatic stress. We reduce the slip weakening distance by factors of 3 and 15 to 0.005 and 0.001 m, respectively. The smaller slip weakening distance is small enough that stress drops to the sliding stress. The maximum acceleration is $\sim$15 m/s^2.

[22] An actual rupture in the shallow subsurface is three-dimensional. A shallow rupture in general differs from earthquakes caused by static tectonic stresses in the crust where physical rupture starts a small nucleation zone and spreads along a fault surface. In particular, a fracture in the shallow subsurface may lie near the plane of the incident

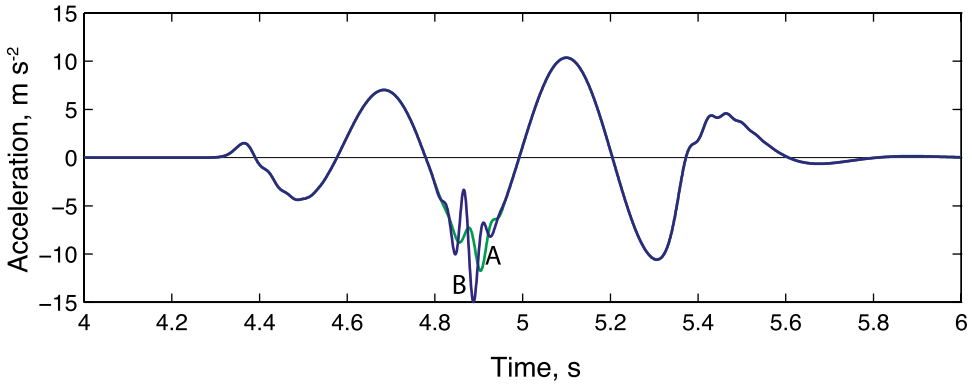

Figure 6. Computed acceleration for a 10 m wide fault at 10 m depth. The seismic velocity, incident wave, and density are the same as in Figures 4 and 5. The slip weakening distance (0.005 m), failure stress, and sliding stress are 1/3 of those in Figures 4 and 5 in curve A, which has a small acceleration pulse. Curve B retains these parameters but has a slip weakening distance of 0.001 m and produces a significant acceleration pulse.

seismic waves. Rupture can nucleate at multiple points where dynamic stresses exceed the strength of the fracture. However, we do not attempt to fit the shape of the FZ16 acceleration pulse as we have only a record from a single station and no other constraints on where a zone of secondary shallow rupture might be.

3.3. Locking Elastic Rheology

[23] A purely elastic material acts nonlinearly if the stress depends nonlinearly on strain. A familiar example is soft shocks of a car driven off road. The riders experience high acceleration when the shocks hit their stops. A jigsaw puzzle is an example relevant to rocks with compliant joints. The puzzle deforms easily until the pieces lock. That is, fractures and joints give compliancy to a rock like the sandstone at FZ 16. These crack-like features deform easily with small strains but asperities come into contact with larger strains. The strong asperities lock the crack, stiffening the rock mass (Figure 7). We are not aware of a laboratory experiment where a rock mass behaved in this manner.

[24] However, an analogous process is better known in rock mechanics [*Jaeger et al.*, 2007, p. 372ff]. Finite shear strain within rocks brings asperities into contact. Further shear strain causes friction and dilatancy as the asperities slide over each other.

[25] We represent this process as purely elastic and assume a vertically propagating SH-wave for simplicity. The stress-strain curve needs to be smooth for numerical stability, and linear at small strains. We use a simple constitutive law with these properties to provide examples,

$$\tau = G_0\varepsilon\left[1+\left(\frac{\varepsilon}{\varepsilon_0}\right)^N\right], \tag{6}$$

where G_0 is the shear modulus at small strains, ε is strain, ε_0 is the strain where the terms in the bracket are equal, and N is a positive even integer (Figure 7). The "tangent" modulus is

$$\frac{d\tau}{d\varepsilon} = G_0\left[1+(N+1)\left(\frac{\varepsilon}{\varepsilon_0}\right)^N\right]. \tag{7}$$

The local seismic velocity depends on the square root of the term in the bracket. The strain energy per volume is

$$\int_0^{\varepsilon}\tau d\varepsilon_d = G_0\varepsilon^2\left[\frac{1}{2}+\frac{1}{N+2}\left(\frac{\varepsilon}{\varepsilon_0}\right)^N\right], \tag{8}$$

where ε_d is a dummy variable for strain. A large value of N implies a sudden increase in stiffness as the strain approaches ε_0. Conversely (8) indicates that a small value of N implies that the nonlinear part of the stiffness (second term in brackets) stores elastic energy over a range of strains.

[26] In comparison, the dynamic stress increases with dynamic strain in the widely used Masing behavior for soils, but the tangent modulus decreases with strain [e.g., *Kramer*, 1996, pp. 240–243; *Hartzell et al.*, 2004]. The unloading curve differs from the loading curve causing hysteresis and nonlinear attenuation. Note that

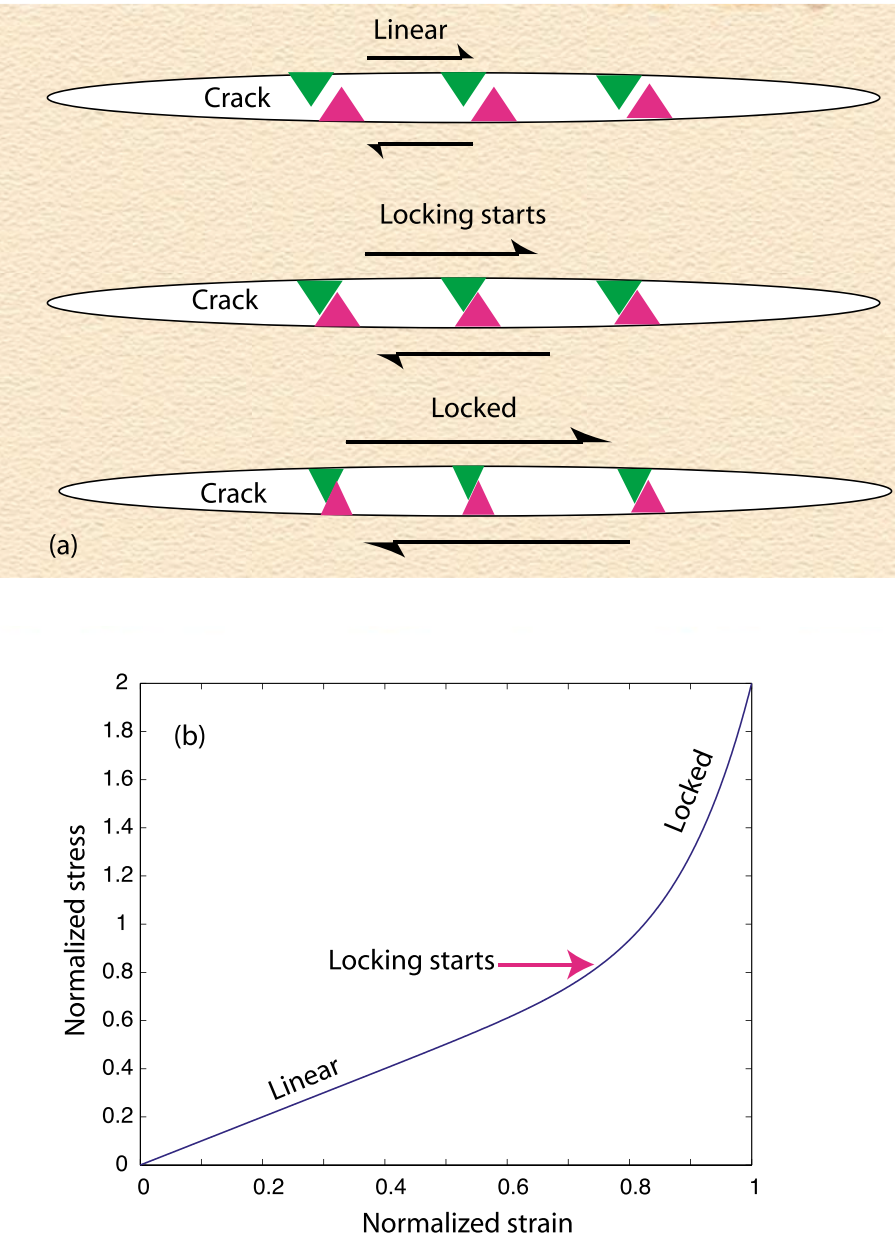

Figure 7. (a) Schematic diagram of compliant crack within stiff rock mass and (b) the resulting stress as a function of strain in units of $\varepsilon/\varepsilon_0$ with $N = 8$. Asperities within the crack do not come into contact at small strains. The rock mass is compliant, and stress depends linearly on strain. Further strain brings asperities into contact and locks the crack. The slope of the curve is the tangent modulus, and the area under the curve is the strain energy per volume.

Elgamal et al. [2005] observed a factor of ~2 increase of the tangent shear modulus at high strains in dense loose saturated sand along with significant hysteresis. We do not attempt to model the response of this complicated rheology. Our models do not include attenuation for simplicity.

[27] We express computed results in normalized units where the period is 1 and use the normalized strain $\varepsilon/\varepsilon_0$ in the upcoming pulse to express amplitude. We plot the computed velocity (Figure 8) and acceleration (Figure 9) for a model with $N = 8$ and the strain amplitude of the initial pulse equal to a minute fraction of ε_0, and factors of 0.398 (curve A), 0.446 (curve B), and 0.486 (curve C) of ε_0. The maximum strains at the quarter-wavelength depth are ~2 times these numbers. That is, they are in the range $\varepsilon/\varepsilon_0 \approx 1$ where the nonlinear term is significant (Figure 7). Computations for lower

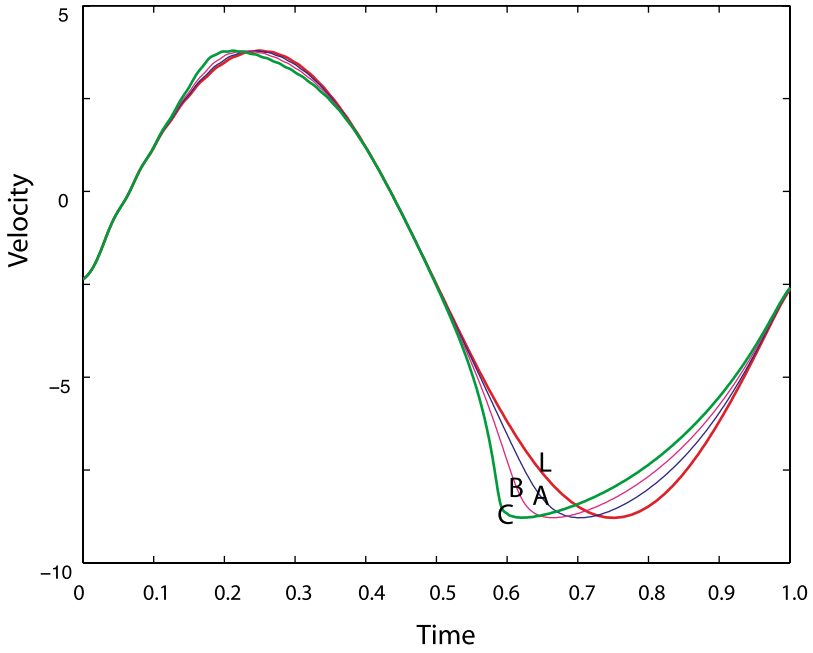

Figure 8. Computed particle velocity versus time for a simple incident pulse. Time is normalized to the period of the pulse. The velocity pulses are normalized so that all the curves would be the same for a linear response. The ratio of ε to ε_0 of the incident wave is 0.398 (curve A), 0.446 (curve B), and 0.486 (curve C). Curve L is the linear response. Note that brief high acceleration occurs around the normalized time of 0.6.

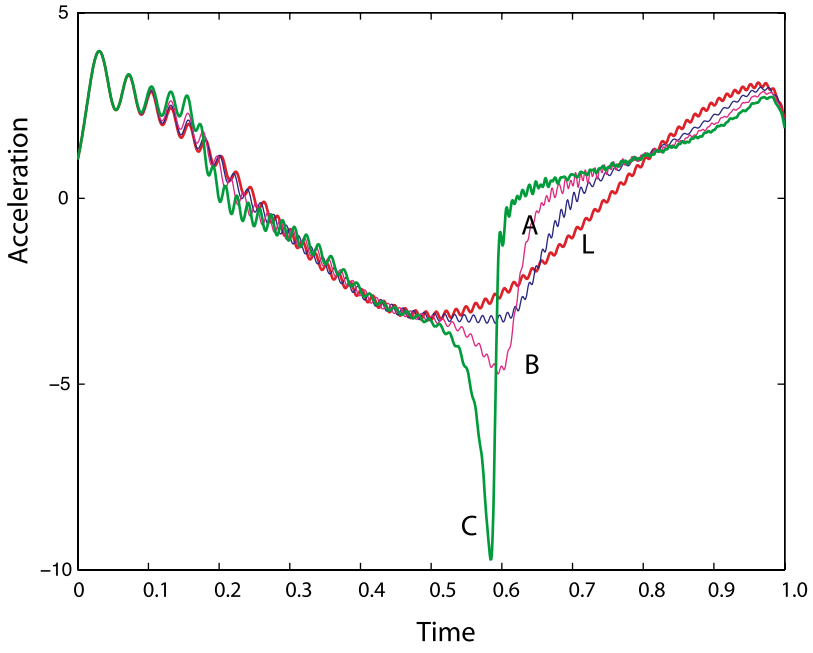

Figure 9. Computed particle acceleration versus time for a simple incident pulse in Figure 8. Time is normalized to the period of the pulse. The acceleration pulses are normalized so that all the curves would be the same for a linear response. The ratio of ε to ε_0 of the incident wave is 0.398 (curve A), 0.446 (curve B), and 0.486 (curve C). Curve L is the linear response. Note that brief high acceleration occurs around the normalized time of 0.6. The high-frequency wiggle owes to numerical dispersion at the highest frequencies. See Appendix A for details.

values of N had this nonlinear behavior at somewhat lower normalized amplitudes $\varepsilon/\varepsilon_0$ of the initial pulse. The maximum "tangent" seismic velocity is less than twice the linear velocity in these models in the range of numerical stability. That is, the tangent shear modulus needs to increase by a factor of ~4 for extreme accelerations to occur. See Appendix A for more discussion of the numerical method.

[28] The amplitude of the velocity pulse is not changed much by the nonlinear elasticity (Figure 8). This is expected since the (conserved) energy in a seismic wave depends on the square of its velocity [e.g., *Timoshenko and Goodier*, 1970, p. 491]. Acceleration pulses are evident later in the record (Figure 9). As already noted, they originate when the upcoming late part of the pulse encountered the reflected pulse at the quarter-wavelength depth (Figure 3).

4. Implications and Conclusions

[29] Seismologists have observed numerous pulses of brief extreme ~2 g acceleration. These arrivals appear only on a small fraction of strong motion records, raising skepticism about their reality. It is, however, productive to seek physically realizable but uncommon subsurface mechanisms. We examined spatially isolated site-specific examples. We constrained physical reasonability by quantifying the nonlinearity needed to produce extreme ground accelerations.

[30] In general, nonlinear behavior of the shallow subsurface can convert low-frequency seismic waves to high-frequency seismic waves. We considered two viable end-member processes: (1) The shallow subsurface fails by faulting driven by dynamic stress carried by seismic waves. Extreme accelerations resulted when rupture occurred near the quarter-wavelength depth of the incident wave on a rupture plane with dimensions comparable to that depth. The dynamic sliding stress was a small fraction of the stress that initiated slip. (2) The rock has a nonlinear rheology. At small strains, open cracks make the rock compliant and linearly elastic. Large strains bring asperities within the cracks into contact, locking them. The rock becomes progressively stiffer with increasing strain. Extreme accelerations occurred when the instantaneous S-wave velocity increased by a factor of ~2 and the shear modulus increased by a factor of ~4 toward that of nearly intact rock. The former process is already known to produce small high-frequency events [*Fischer et al.*, 2008; manuscript in preparation, 2008]. A combination of the two processes is attractive where locking of cracks leads to high dynamic stress and then faulting.

[31] Both processes require that the shallow subsurface is able to store and then quickly release elastic strain energy. Fractured bedrock as at the FZ 16 station has this property as the intact domains are stiff and there are well-defined fractures that may either lock or become faults (Figure 3). Intuitively, near-total stress drops are likely at shallow depths; once the locking asperities fail a nearly open fracture may behave like a free surface.

[32] A predictable feature of our nonlinear mechanisms is that the highest accelerations occur well into the pulse after the reflected waves interact with the remaining upcoming waves (Figure 3). In contrast, the highest accelerations from a "burst" of energy on the main earthquake fault occur at the start of the pulse [*Brune*, 1970]. A borehole or surface array would help to resolve the radiation pattern and depth of a secondary source as well as a primary source on the main fault.

[33] Rupture and locking are local on the scale of the wavelength of incident wave. Vagaries in the strength of throughgoing fracture planes, their tendency to stick-slip or lock, and likely fractal pre-stress [see *Marsan*, 2005] of the shallow subsurface make the precise locations of rupture and locking and consequent sites of brief extreme acceleration unpredictable and perhaps unrepeatable between subsequent episodes of strong ground motion. It is unproductive to model the details of a record from a single station without more information.

[34] Some engineering implications of our testable hypothesis are obvious. Brief pulses of extreme acceleration occur, but imply that the total energy arriving at a structure was redistributed and attenuated. Significantly stronger incident waves would encounter nonlinear attenuation before they shock the surface. They do not imply that sustained very extreme accelerations are likely, as they are not generated on the main fault plane. As already noted, brief pulses of extreme acceleration do not endanger reasonably constructed structures [e.g., *Kramer*, 1996, p. 68].

Appendix A: Numerical Method

[35] We use an explicit numerical method to compute ground time histories at the surface for our

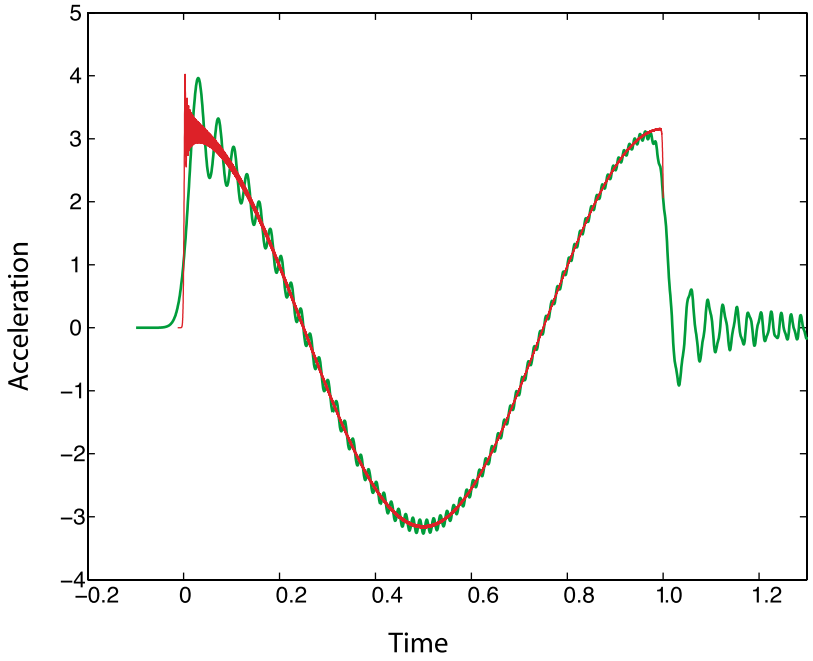

Figure A1. Check of the numerical method for computing acceleration for the linear response in Figure 9. The wiggly curve samples the pulse with 1000 intervals, while the smoother pulse has 16000 intervals. The dispersion still exists in the well-sampled model, but the example shows that the method converges and the average acceleration is a good representation of the actual quantity. A smoother initial pulse or filtering would cloak the artifact.

upcoming pulse started at depth. Our method leads to easily understood numerical artifacts. We could use a more sophisticated method to model linear elasticity, but the artifacts with nonlinear elasticity then would be difficult to analyze.

[36] We have displacement nodes defined at each depth numbered down from the free surface that we update at successive time steps by equating forces and acceleration. We use dimensionless units where the linear shear modulus, the density, and the grid spacing are all 1. The time step is Δt. We define shear stresses halfway between our displacement nodes. The shear traction above an example grid node i is

$$\tau_{\mathrm{up}} = F(D_i - D_{i-1}), \tag{A1}$$

where D is displacement and F is a function of the form of (6) normalized so that it is $D_i - D_{i-1}$ for small values of this parameter. The stress below the node is

$$\tau_{\mathrm{down}} = F(D_{i+1} - D_i). \tag{A2}$$

The force-acceleration balance equation is

$$\tau_{\mathrm{down}} - \tau_{\mathrm{up}} = \frac{(D_{\mathrm{old}} + D_{\mathrm{new}} - 2D)_i}{\Delta t^2}, \tag{A3}$$

where the subscript old indicates the value from the previous time step and new the value from the next time step. All the displacements in the acceleration term are evaluated at node i; we solve for the new displacement at each node.

[37] For linear elasticity, this scheme is stable for $\Delta t \leq 1$ and it exactly yields the kinematic wave solution in a constant normalized velocity $V = 1$ medium for $\Delta t = 1$. With nonlinear elasticity, the seismic velocity increases with strain. We let $\Delta t = 0.5$, which is stable if the normalized velocity is less than 2.

[38] This time interval $\Delta t = 0.5$, however, causes dispersion at high frequencies and short wavelength, which are present in our model because the acceleration in (5) is discontinuous at the start and end of our pulse. We do not impose a smooth start and end to the signal, which would conceal this feature of the code. The high frequencies propagate at a slower velocity than the main pulse and are evident in the acceleration plot but not the velocity plot. We refined our grid from 1000 to 16000 intervals in the pulse (Figure A1). Our method converges to the expected kinematic pulse in the limit of infinite nodes, but dispersion still occurs at the shortest wavelength. The computed acceleration oscillates about the expected result

indicating that the velocity as the integral of acceleration is well resolved. The dispersion causes a short wavelength to lag the main signal. It cannot cause sharp pulses of extreme acceleration. We plotted curves with 1000 points in the pulse. Curves with very large numbers of nodes proved difficult to plot electronically.

[39] To start the numerical calculation, we define displacement at two consecutive time steps. It is numerically easier to start a pulse within a constant velocity linear medium. Hence, we confined nonlinear elasticity to the region above the starting pulse. Otherwise, we model a half-space. As noted, nonlinear effects are strong only near the quarter wavelength depth.

Acknowledgments

[40] This research was in part supported by NSF grant EAR-0406658 and by the Southern California Earthquake Center (SCEC). SCEC is funded by NSF Cooperative Agreement EAR-0106924 and USGS Cooperative Agreement 02HQAG0008. The SCEC contribution number for this paper is 1144. We thank Adam Fischer and Charles Sammis for preprints of their papers and helpful discussions at the 2007 SCEC annual meeting. Greg Beroza critically read the manuscript.

References

Andrews, D. J. (1999), Test of two methods for faulting in finite-difference calculations, *Bull. Seismol. Soc. Am.*, *89*, 931–937.

Brune, J. N. (1970), Tectonic stress and the spectra of seismic shear waves from earthquakes, *J. Geophys. Res.*, *75*, 4997–5009.

Elgamal, A., Z. Yang, T. Lai, B. L. Kutter, and D. W. Wilson (2005), Dynamic response of saturated dense sand in laminated centrifuge container, *J. Geotech. Geoenviron. Eng.*, *131*(5), 598–609.

Fischer, A. D., C. G. Sammis, Y. Chen, and T.-L. Teng (2008), Dynamic triggering by strong motion P- and S-waves: Evidence from 1999 Chi-Chi, Taiwan Earthquake, *Bull. Seismol. Soc. Am.*, in press.

Hartzell, S., L. F. Bonilla, and R. A. Williams (2004), Prediction of nonlinear soil effects, *Bull. Seismol. Soc. Am.*, *96*, 1609–1629.

Jaeger, J. C., N. G. W. Cook, and R. W. Zimmerman (2007), *Fundamentals of Rock Mechanics*, 4th ed., 475 pp., Blackwell, Malden, Mass.

Kramer, S. L. (1996), *Geotechnical Earthquake Engineering*, 653 pp., Prentice-Hall, Upper Saddle River, N. J.

Ma, S., S. Custódio, R. J. Archuleta, and P. Liu (2008), Dynamic modeling of the 2004 M_w 6.0 Parkfield, California, earthquake, *J. Geophys. Res.*, *113*, B02301, doi:10.1029/2007JB005216.

Marsan, D. (2005), The role of small earthquakes in redistributing crustal elastic stress, *Geophys. J. Int.*, *163*, 141–151.

Shakal, A. F., H. R. Haddadi, and M. J. Huang (2006), Note on the very-high-acceleration Fault Zone 16 record from the 2004 Parkfield earthquake, *Bull. Seismol. Soc. Am.*, *96*, S119–S128.

Timoshenko, S. P., and J. N. Goodier (1970), *Theory of Elasticity*, 567 pp., McGraw-Hill, New York.